Published in final edited form as:
J Biol Chem. 2002 December 27; 277(52): 50725–50733. doi:10.1074/jbc.M204159200.

Protection from Pancreatitis by the Zymogen Granule Membrane Protein Integral Membrane-associated Protein-1*

Takuji Imamura[‡], **Minoru Asada**[‡], **Sherri K. Vogt**, **David A. Rudnick**, **Mark E. Lowe**, and **Louis J. Muglia**[§]
Departments of Pediatrics, Molecular Biology and Pharmacology, and Obstetrics and Gynecology, Washington University School of Medicine and St. Louis Children's Hospital, St. Louis, Missouri 63110

Abstract

Pancreatitis is a common disease with substantial morbidity and mortality. To better understand the mechanisms conferring sensitivity or resistance to pancreatitis, we have initiated the analysis of novel acinar cell proteins. Integral membrane-associated protein-1 (Itmap1) is a CUB (complement subcomponents C1r/C1s, sea urchin Uegf protein, bone morphogenetic protein-1) and zona pellucida (ZP) domain-containing protein we find prominently expressed in pancreatic acinar cells. Within the acinar cell, Itmap1 localizes to zymogen granule membranes. Although roles in epithelial polarity, granule assembly, and mucosal protection have been postulated for CUB/ZP proteins, *in vivo* functions for these molecules have not been proven. To determine the function of Itmap1, we generated Itmap1-deficient mice. *Itmap1*$^{-/-}$ mice demonstrate increased severity of secretagogue- and diet-induced pancreatitis in comparison to *Itmap1*$^{+/+}$ mice. In contrast to previous animal models exhibiting altered severity of pancreatitis, Itmap1 deficiency results in impaired activation of trypsin, an enzyme believed critical for initiating a cascade of digestive zymogen activation during pancreatitis. Itmap1 deficiency does not alter zymogen granule size, appearance, or the composition of zymogen granule contents. Our results demonstrate that Itmap1 plays an essential role in trypsinogen activation and that both impaired and augmented trypsinogen activation can be associated with increased severity of pancreatitis.

Acute pancreatitis remains a significant cause of morbidity and mortality in the United States (1, 2). These attacks often require hospitalization, and ~10% of patients die. The treatment of pancreatitis centers on supportive care coupled with close observation for complications. No therapy alters the course of acute pancreatitis. The lack of therapy stems, at least in part, from a paucity of information about the events that led to pancreatic inflammation.

Virtually all theories about the pathogenesis of acute pancreatitis have included autodigestion of the pancreas by the digestive enzymes normally synthesized in the pancreatic acinar cells (1, 2). In these models, some event triggers the inappropriate release of digestive enzymes into the parenchyma of the pancreas. Whatever the trigger, most authors believe that the insult causes the premature activation of trypsinogen to trypsin

*This work was supported by grants from the March of Dimes, Burroughs Wellcome Fund, and National Institutes of Health Grants AA12957 (to L. J. M.) and DK52574 (to M. E. L.). The costs of publication of this article were defrayed in part by the payment of page charges. This article must therefore be hereby marked "*advertisement*" in accordance with 18 U.S.C. Section 1734 solely to indicate this fact.

§To whom correspondence should be addressed: Washington University School of Medicine, Box 8208, 660 S. Euclid Ave., St. Louis, MO 63110. Tel.: 314-286-2847; Fax: 314-286-2893; Muglia_L@kids.wustl.edu.
‡Both authors contributed equally to this work.

within the acinar cell. As trypsin accumulates, it activates other proenzymes (zymogens), and the combined action of these proteases and lipases further damages the pancreas.

Several recent studies support the central role of trypsinogen activation in the pathophysiology of pancreatitis. Most patients with hereditary pancreatitis have a mutation in the gene encoding cationic trypsinogen (3). The mutation may allow trypsin to accumulate in the acinar cell and activate other digestive enzymes. Studies with mice deficient in cathepsin B, a lysosomal hydrolase that can convert trypsinogen to trypsin, support the importance of trypsinogen activation and the fusion of lysosomes and zymogen granules in the pathophysiology of pancreatitis (4). The cathepsin B-deficient mice have decreased edema and cellular necrosis associated with decreased trypsinogen activation in an experimental model of pancreatitis induced by hyperstimulation with cerulein.

To protect the pancreas from the inappropriate activation of trypsinogen and other zymogens, mechanisms have evolved that maintain the integrity of the pancreas (5). These mechanisms include the synthesis and secretion of digestive enzymes as inactive zymogens, the synthesis of protease inhibitors, the compartmentalization of proenzymes in specialized zymogen granules destined for trafficking to the apical plasma membrane, and the activation of proenzymes in the duodenum. Together, these protective mechanisms prevent or limit the cascade of proenzyme activation that results in tissue damage. For acute pancreatitis to develop, these protective mechanisms must fail and permit the untimely activation of digestive enzymes by trypsin.

Only in the rare patient with hereditary pancreatitis is there a clue as to how the protective mechanisms might fail in acute pancreatitis (3). For the majority of patients with acute pancreatitis no mechanism is known. Other factors must predispose to premature trypsinogen activation or, alternatively, entirely distinct mechanisms may lead to pancreatitis in these patients. Further insight into these mechanisms may lead to novel strategies for identifying individuals at risk for pancreatitis and to more effective therapies for this potentially lifethreatening disorder.

To further understand the mechanisms involved in protecting the acinar cell from digestive damage, we have evaluated the function of a novel acinar cell zona pellucida (ZP)[1] domaincontaining protein Itmap1 (6). ZP domain proteins such as uromodullin, the pancreatic ductal protein muclin, the zymogen granule protein GP2, and the inner ear protein β-tectorin are often found in fibrillar or gelatinous compartments of the extracellular matrix, with the ZP domain serving as a filament-organizing motif (7). This filamentous structure may contribute to mucosal protection by providing barrier function. Alternatively, ZP domain proteins have also been implicated in trafficking of secretory granules in the pancreas (8). In this study, we demonstrate that Itmap1 is a protein tightly associated with zymogen granule membranes and that Itmap1 attenuates the severity of pancreatitis.

EXPERIMENTAL PROCEDURES

Generation of Itmap1$^{-/-}$ Mice

We isolated an 861-bp cDNA encoding Itmap1 using gestation day 16 uterus poly(A)$^+$ RNA as “tester” and gestation day 19 poly(A)$^+$ RNA as “driver” in a PCR-Select cDNA

[1]The abbreviations used are: ZP, zona pellucida; CDE, choline-deficient, ethionine-supplemented; CUB, complement subcomponents C1r/ C1s, sea urchin Uegf protein, bone morphogenetic protein-1; ES, embryonic stem; Itmap1, integral membrane-associated protein-1; IEF, isoelectric focusing; MPO, myeloperoxidase; TAP, trypsinogen activation peptide; PBS, phosphate-buffered saline; MOPS, 4-morpholinepro-panesulfonic acid; MES, 4-morpholineethanesulfonic acid; CHAPS, 3-[(3-cholamidopropyl)dimethylammonio]-1-propanesulfonic acid; TUNEL, terminal deoxynucleotidyl transferase-mediated dUTP nick end labeling.

subtraction kit (Clontech, Palo Alto, CA). Random-primer-labeled fragments of the Itmap1 cDNA were used to screen a murine 129Sv genomic DNA library (Stratagene, La Jolla, CA). Two genomic clones were isolated and used for sequence analysis and identification of intronexon boundaries.

To generate the vector for homologous recombination, a 3.3-κb *Xba*I-*Eco*RI fragment beginning in intron 1 was first cloned into *Xba*I- and *EcoR*I-digested pPNT (9) to generate pPNT.Itmap1–3'. Next, the 3.8-κb *Not*I-*BamH*I fragment ending 1.6-κb 5' to the transcription initiation site was excised from pBluescript SK II + as a *Not*I-*Xho*I fragment and cloned into pPNT.Itmap1–3' to generate the final targeting vector pPNTΔItmap1. The TC1 line of embryonic stem (ES) cells (10) underwent electroporation with linearized pPNTΔItmap1 and selection as previously described (11). ES clones having undergone appropriate homologous recombination were identified by Southern blot analysis employing a 240-bp *EcoR*I-*BamH*I probe external to the *Itmap1* genomic sequences in the targeting vector. Two independent clones were selected for blastocyst injection, each of which proved capable of germ line transmission. Mice used for these experiments were of a mixed 129 × Black Swiss background; similar results have been obtained on mice of mixed 129 × C57BL/6 or inbred 129SvJ backgrounds.

Immunohistochemistry

A 488-bp cDNA fragment extending from nucleotide 1048 to 1535 of the Itmap1 cDNA (GenBank™ accession number U69699) was cloned into the *Xho*I and *Kpn*I sites of the bacterial expression vector pBAD/HisC (Invitrogen, Carlsbad, CA) for generation of a recombinant protein fragment. After purification from arabinose-induced bacteria, the protein fragment was injected into two rabbits for generation of anti-Itmap1 polyclonal antisera. Serum from rabbit 67418 was utilized for the current studies at a dilution of 1:5000 on paraformaldehyde-fixed, paraffin-embedded tissues cut at 5 μm. Antibody binding was visualized with a goat anti-rabbit Cy3 secondary antibody. Sections were counterstained with 4',6-diamidino-2-phenylindole for localization of cell nuclei.

In Situ Hybridization

Tissues were fixed by immersion in diethylpyrocarbonate-treated 4% paraformaldehyde in PBS for 24 h at 4 °C. Samples were then cryopreserved in 10% sucrose in PBS, and embedded in OCT compound (Miles, Elkhart, IN) for sectioning on a cryostat. 14-μm sections were thaw-mounted onto Superfrost Plus slides (Fisher Scientific, Pittsburgh, PA) and hybridized to an [α-^{33}P]UTP-labeled 861-base Itmap1 riboprobe as previously described (12). After washing, slides were exposed to Kodak NTB-2 emulsion (Eastman Kodak Co., Rochester, NY) for 3–10 days and developed. Immediately adjacent slides were counterstained with hematoxylin and eosin.

Electron Microscopy

For ultrastructural analysis, pancreata were minced into 1-mm^3 pieces, immersion-fixed in 2.5% glutaraldehyde in 0.1 M sodium cacodylate buffer at 4 °C overnight, and postfixed in 1.25% osmium tetroxide. Samples were thin-sectioned in Polybed 812 (Polysciences, Warrington, PA), poststained with uranyl acetate and lead citrate, and visualized on a Zeiss 902 microscope (Zeiss, Thornwood, NY). For immunoelectron microscopy, pancreata were fixed in 8% paraformaldehyde-PBS overnight at 4 °C, rinsed three times in PBS, infused in 2 M sucrose-polyvinylpyrrolidone, and processed for ultracryotomy. Ultrathin sections were prepared and incubated with blocking buffer containing 10% goat serum. Immunolabeling was done by incubating with the anti-Itmap1 antibody for 2 h, followed by secondary antibody (12-nm-gold-labeled goat anti-rabbit) for 1 h. After washing, sections were stained

with uranyl acetate and embedded in methyl cellulose. Specimens were visualized with a Zeiss 902 microscope, and photographs were recorded with Kodak EM film.

Zymogen Granule Enrichment

Pancreatic acinar cell zymogen granules were prepared from adult mice as previously described (13, 14). Two to three pancreata were placed in ice-cold 250 mM sucrose, 5 mM MOPS (pH 7.0), 0.1 mM $MgSO_4$ containing one MiniComplete tablet (Roche Molecular Biochemicals, Indianapolis, IN) per 10 ml of buffer. The pancreata were homogenized for 30 s with a Polytron on setting 8000 followed by four strokes with a loose-fitting glass Dounce homogenizer. The mixture was centrifuged at 150 × *g* for 15 min, and the supernatant was re-centrifuged at 1300 × *g* for 15 min. The pellet was mixed with 40% Percoll, 250 mM sucrose, 50 mM MES (pH 5.5), 0.1 mM $MgSO_4$, 2 mM EGTA, and one MiniComplete tablet per 10 ml. The zymogen granules were banded by centrifugation at 100,000 × *g* for 20 min. The zymogen granules were washed by dilution with homogenization buffer and centrifugation at 1300 × *g* for 10 min. The granules were osmotically lysed and the membranes isolated and washed as described (14). The first post-lysis supernatant containing the granule contents was also saved for analysis. Enrichment of zymogen granule contents and membranes was confirmed determining the relative abundance of amylase in each preparation by Western blot analysis with an anti-amylase primary antibody (data not shown).

RNA and Protein Analyses

Ten micrograms of total RNA was subjected to electrophoresis through 1.2% agarose-formaldehyde gels and transferred to nitrocellulose membranes. [α-^{32}P]UTP-labeled RNA probes specific for mouse Itmap1 mRNA, cyclophilin mRNA, or 18 S ribosomal RNA were hybridized at 60 °C in 50% formamide-containing buffer as previously described (15).

Total cellular membrane proteins and zymogen granule membrane proteins and contents were subjected to 8% SDS-PAGE electrophoresis and then transferred to nitrocellulose membranes. Itmap1 was detected with our rabbit anti-Itmap1 primary antibody used at a 1:2000 dilution (total membrane proteins) or 1:5000 dilution (zymogen granule-enriched membranes and contents) and visualized using an enhanced chemiluminescent detection kit (Amersham Biosciences, Arlington Heights, IL). Zymogen granule glycoproteins were detected with perox-idase-conjugated concanavalin A and wheat-germ agglutinin after electrophoretic separation and transfer to nitrocellulose membranes (16). Ponceau S staining of membranes confirmed equivalent protein loading and transfer. Carbohydrate residues were removed from zymogen granule membrane glycoproteins by digestion with peptide: *N*-glycosidase F according to the manufacturer's recommended protocol (New England BioLabs, Inc., Beverly, MA). For Pronase digestion the zymogen granules were isolated and washed as above except that the last wash did not contain protease inhibitors. The granules were suspended in 1.0 ml of wash buffer divided into four 300-μl aliquots. The granules were incubated on ice for 10 min in buffer alone, buffer with 7% Nonidet P (NP)-40, buffer with 0.33 unit of Pronase, and buffer with 7% Nonidet P-40 and 0.33 unit of Pronase. The reaction was stopped by adding 700 μl of SDS-sample buffer containing one MiniComplete tablet (Roche Molecular Biochemicals, Indianapolis, IN) per 10 ml of buffer followed by boiling for 5 min.

Two-dimensional Gel Electrophoresis

Forty micrograms of protein from zymogen granule contents were diluted in rehydration solution (Amersham Biosciences, Piscataway, NJ) containing 8 M urea and 2% CHAPS and loaded onto pH 3–10 gradient isoelectric focusing (IEF) strips for first-dimension separation on the basis of IEF point. Samples were focused for ~12,000 V-h to equilibrium. The

focused samples were then loaded onto 4–12% gradient acrylamide gels for second dimension separation by SDS-PAGE on the basis of size. Gels were stained with Coomassie Brilliant Blue G-Colloidal (Sigma, St. Louis, MO). Individual protein spots on scanned images were quantitated densitometrically using Scion Image (Scion Corp., Frederick, MD) software from replicate gels.

Pancreatitis Induction

For cerulein-induced pancreatitis (17–19), 2- to 3-month-old male *Itmap1*$^{+/+}$ and *Itmap1*$^{-/-}$ mice were injected with seven doses of either 50 μg/kg cerulein in normal saline or normal saline at hourly intervals following an overnight fast and *ad libitum* access to water. 8 h (vehicle and cerulein-injected mice) and 24 h (cerulein-injected mice) after the initial injection, blood was obtained by retro-orbital phlebotomy for measurement of amylase and lipase activity on a Vitros 250 analyzer (Ortho Clinical Diagnostics, Rochester, NY) using reagents supplied by the instrument manufacturer (n = 6–9 per group). 8 h after the initial injections, an additional n = 4–6 mice were euthanized, and their pancreata were isolated and weighed. Pancreata were then immersion-fixed in 4% paraformaldehyde, embedded in paraffin, cut into 5-μm sections, and stained with hematoxylin and eosin. Photographs of coded sections (4–6 fields per mouse) were examined by two independent observers and scored for necrosis using the following semi-quantitative scale: 0, no necrosis; 1, periductal necrosis (<5%); 2, focal necrosis (5–20%); 3, diffuse parenchymal necrosis (>20%). Additional sections were evaluated for acinar cell apoptosis by TUNEL-staining employing an Apoptag peroxidase kit (Intergen Co., Purchase, NY). Sections were counterstained with methyl green after the peroxidase reaction. Quantitation of apoptotic cells was performed on n = 4 saline-treated mice and n = 4–5 cerulein-treated mice. The average number of apoptotic nuclei per ×400 field was calculated from three (saline) or eight (cerulein) random, independent fields per mouse.

For the measurement of intra-pancreatic enzyme activities, the pancreas was removed at the indicated times after initiation of cerulein injections and immediately frozen in liquid nitrogen and stored at −80 °C. For the measurement of trypsin activity, the tissue was thawed and homogenized in ice-cold 5 mM MOPS (pH 6.5), 1 mM $MgSO_4$, and 250 mM sucrose (4). The sample was sonicated for 30 s and centrifuged for 5 min at 16,000 × *g*. The same buffer supplemented with 1 mM EDTA and 0.1% Triton X-100 was used to prepare the sample for assay of the trypsinogen activation peptide (TAP). After homogenization, the sample was boiled for 10 min, and a supernatant was prepared by centrifugation at 16,000 × *g* for 5 min. For myeloperoxidase (MPO) assays, pancreatic tissue was homogenized in 20 mM potassium phosphate (pH 7.0) and centrifuged for 10 min at 10,000 × *g* (4). The pellet was resuspended in 50 mM potassium phosphate buffer (pH 6.0) containing 0.5% cetyltrimethylammonium bromide. Afterward the sample was frozen and thawed four times and sonicated for 10 s, and the supernatant was prepared by centrifugation at 10,000 × *g* for 5 min. Protein concentrations in the samples were determined by the BCA method (Pierce, Rockford, IL). Trypsin, TAP, and MPO were measured by published methods (4). Relative amounts of trypsinogen were determined by protein immunoblot of pancreatic extracts with a rabbit polyclonal antibody against trypsinogen (Abcam Ltd., Cambridge, UK). Relative abundance of trypsinogen on scanned immunoblots was determined by densitometric analysis with results expressed as normalized absorbance/mg of total protein. Cathepsin B activity was determined with α-*N*-benzyloxycarbonyl-Arg-Arg-β-naphthylamide as described previously (20). Cathepsin B activity is reported as relative units (change in fluorescence/min)/mg of total protein. Each assay was done in triplicate on samples isolated from three different mice of each genotype at each time point. To evaluate cerulein-induced signaling in pancreata from mice of each genotype, the cerulein concentration dependence of

amylase secretion from pancreatic snips harvested 1–2 h prior to stimulation was measured in triplicate as previously described (21).

Diet-induced pancreatitis was precipitated by placing 2- to 3-month-old *Itmap1*$^{+/+}$ (n = 17) and *Itmap1*$^{-/-}$ (n = 18) female mice (body weight, 25 ± 0.5 g) on choline-deficient, 0.5% ethionine-supplemented (CDE) chow (Dyets, Inc., Bethlehem, PA) as previously described (22, 23). We chose to test this age range of mice, because they are somewhat more resistant to morbidity in this model of pancreatitis. After an overnight fast, mice received the CDE chow for 48 h and then were returned to normal rodent chow. Samples for serum enzymes (n = 8 per genotype) and pancreatic histology (n = 3 per genotype) were obtained 72 h after the initiation of the CDE diet.

Statistical Methods

All results are expressed as mean ± S.E. unless otherwise indicated. Statistical analysis was by analysis of variance, with $p \leq 0.05$ considered significant. Differences in mortality were assessed for significance by Chi-square analysis. Statistical analysis of the semi-quantitative assessment of acinar cell necrosis was by Mann-Whitney rank sum.

RESULTS

In Vivo Expression of Itmap1

Itmap1 was first identified as a novel ZP protein induced specifically in late gestation mouse uterus (6). In accord with this previous report, we found no expression of Itmap1 in non-gravid mouse uterus and high level expression in mid-to-late gestation uterus (Fig. 1*a*). Within the uterus, Itmap1 expression localized exclusively to the epithelium (Fig. 1*b*). A general tissue survey in non-gravid mice was notable for high levels of Itmap1 expression in the pancreas, a site not previously evaluated for Itmap1 expression. *In situ* hybridization to histological sections of pancreas demonstrated Itmap1 mRNA expression in acinar cells but not ductal epithelium (Fig. 1*c*). Other tissues, including spleen, stomach, kidney, thymus, ileum, and colon did not express Itmap1 mRNA (data not shown).

Subcellular Localization of Itmap1

To define the cellular distribution of Itmap1, we generated a rabbit polyclonal antiserum against the junction of the CUB and ZP domains of Itmap1. By immunofluorescence, this antiserum detected Itmap1 immunoreactivity throughout the acinar cell population of the pancreas (Fig. 2*a*). The staining co-localized with zymogen granules. We confirmed that Itmap1 resides in the zymogen granules by immunoelectron microscopy (Fig. 2*b*). Grains were only associated with zymogen granules. In the uterus, the anti-Itmap1 antibody also stained granular structures in the apical region of the epithelium (data not shown). This pattern of expression was specific for Itmap1 and not other ZP domain proteins, because *Itmap1*$^{-/-}$ mice (described below) failed to demonstrate any immunoreactivity.

The amino acid sequence of Itmap1 contains a predicted signal peptide and transmembrane domain indicating that Itmap1 should localize to a cellular membrane. To determine if Itmap1 associates with membranes, we performed Western blots on preparations of total membranes and of zymogen granule-enriched membranes from both wild type and *Itmap1*$^{-/-}$ mice. Our antibody detected a strongly positive 110-kDa protein in total cellular membrane preparations from wild type pancreas and uterus (Fig. 3*a*). In contrast, only weak, nonspecific bands were detected in membranes prepared from *It-map1*$^{-/-}$ mice (Fig. 3*a*) and when pre-immune serum was substituted for the anti-Itmap1 antibody (data not shown). A protein of identical size was also present in alkali-extracted zymogen granule-enriched membranes from wild type but not Itmap1-deficient mice (Fig. 3*b*). Itmap1 reactivity was

not present in zymogen granule contents. Thus, Itmap1 is tightly associated with zymogen granule membranes, and, by virtue of its predicted transmembrane domain, likely to be an integral membrane protein.

To determine whether the larger amino-terminal CUB/ZP portion of Itmap1 resides within or outside the zymogen granule, we subjected isolated zymogen granules to protease digestion with or without permeabilization with the detergent Nonidet P-40. Itmap1 immunoreactivity was abolished with Pronase treatment only after permeabilization of the zymogen granules with detergent, demonstrating that the CUB and ZP domains reside within the zymogen granule (Fig. 3*c*).

Because the Itmap1 cDNA sequence predicts a product of 69 kDa and our antiserum recognizes a product of ~110 kDa, we investigated the possibility that post-translational glycosylation of Itmap1 explained the size difference. Western blot analysis of zymogen granule membrane proteins with the anti-Itmap1 antibody after digestion with peptide: *N*-glycosidase F resulted in disappearance of the 110-kDa protein band, and appearance of a new 69-kDa immunoreactive band, confirming that the observed size of mature Itmap1 results from glycosylation (Fig. 3*d*).

Generation and Characterization of *Itmap1*$^{-/-}$ Mice

To determine the role of Itmap1 in zymogen granule function *in vivo*, we generated *Itmap1* mice by homologous recombination in embryonic stem cells. The *Itmap1* gene consists of eight exons encompassing ~13 kb of mouse genomic DNA (Fig. 4*a*). In our targeting vector, we replaced exon 1, encoding the translation start site and first 27 amino acids, and 1.6 kb 5' to the transcription initiation region, with a phosphoglycerate kinase-neomycin resistance cassette (Fig. 4*b*). Two independently targeted clones were selected for microinjection, and both proved capable of germ line transmission. Similar results were obtained with *Itmap1*$^{-/-}$ mice arising from each clone. To ensure that deletion of the *Itmap1* transcription promoter region and exon 1 resulted in a null allele, we performed RNA blot analysis of uterus RNA from gravid mice at 18.5 days of gestation utilizing a hybridization probe detecting mRNA sequences 3' to the deleted region. Robust Itmap1 mRNA expression was found in *Itmap1*$^{+/+}$ mice, and Itmap1 mRNA was absent in *Itmap1*$^{-/-}$ mice (Fig. 4*c*). *Itmap1*$^{-/-}$ mice exhibit normal growth, longevity, and fertility when compared with *Itmap1*$^{+/+}$ litter-mates. *Itmap1*$^{-/-}$ females have normal timing for parturition, reproducibly delivering viable litters at 19.5 days of gestation. Zymogen granule size (*Itmap1*$^{+/+}$ 0.81 ± 0.02 μm versus *Itmap1*$^{-/-}$ 0.78 ± 0.2 μm; $n = 3$ mice per group, 40 granules measured per animal) and appearance by electron microscopy did not differ between *Itmap1*$^{+/+}$ and *Itmap1* mice (Fig. 4*d*).

Recent studies evaluating other pancreatic ZP proteins suggest that they may be involved in the intracellular trafficking of secretory granules and in the regulated exocrine transport of digestive enzymes (8) or play other roles in maintenance of mucosal integrity (24, 25). Based upon its structure and pattern of cellular distribution, we hypothesized that Itmap1 could serve a role in maintaining pancreatic integrity. We initiated our evaluation of possible differences in responses to injury in the pancreas by measuring the severity of cerulein-induced pancreatitis in *Itmap1*$^{+/+}$ and *Itmap1*$^{-/-}$ mice. Repetitive administration of cerulein, a cholecystokinin analogue, induces an acute hyperstimulation pancreatitis associated with elevated serum amylase and lipase concentrations, and interstitial pancreatic edema (17–19). Cerulein-induced pancreatitis caused no mortality in either *Itmap1*$^{+/+}$ or *Itmap1*$^{-/-}$ mice. *Itmap1*$^{-/-}$ mice, however, demonstrated increased severity of pancreatitis histologically, with greater edema causing wider separation between pancreatic lobules and disruption of acini (Fig. 5). The histological appearance of greater edema in the *Itmap1*$^{-/-}$ mice was confirmed by greater pancreatic wet weight after cerulein hyperstimulation (Fig. 6*a*). Semi-

quantitative analyses of necrotic acinar cells indicated a mild increase in necrosis in *Itmap1*$^{-/-}$ compared with *Itmap1*$^{+/+}$ mice ($p = 0.027$; data not shown). Additionally, *Itmap1*$^{-/-}$ mice had significantly increased numbers of apoptotic acinar cells after cerulein treatment in comparison to *Itmap1*$^{+/+}$ controls (Fig. 6 *b*). Analysis of serum amylase and lipase levels (Fig. 6*c*) revealed a statistically significant elevation in basal lipase concentration in the *Itmap1*$^{-/-}$ mice (*Itmap1*$^{+/+}$ 786 ±117 units/ liter *versus Itmap1*$^{-/-}$ 1189 ±112 units/liter; $p < 0.05$). At 8 and 24 h after cerulein administration, lipase levels rose significantly in both groups and were 38 and 56% higher in the *Itmap1*$^{-/-}$ mice when compared with *Itmap1*$^{+/+}$ mice ($p < 0.05$ and $p < 0.005$, respectively), again in accord with greater pancreatic damage. The greater severity of pancreatitis in *It-map1*$^{-/-}$ mice is unlikely to arise from altered intracellular cerulein-induced signaling because pancreatic snips harvested from *Itmap1*$^{-/-}$ and *Itmap*$^{+/+}$ mice show very similar patterns of amylase secretion as a function of cerulein concentration (Fig. 6*d*).

We next determined the response of *Itmap1* mice to the more severe hemorrhagic pancreatitis induced by administration of a choline-deficient, ethionine-containing (CDE) diet (22, 23, 26). The *Itmap1*$^{-/-}$ mice demonstrated greater acinar cell necrosis and tissue edema after 2 days of the CDE diet (Fig. 5). Consistent with the greater degree of histological damage, *Itmap1*$^{-/-}$ mice had markedly elevated serum amylase and lipase levels at the same time (Fig. 6*c*). Finally, the CDE diet was associated with only 53% survival in the *Itmap1*$^{-/-}$ mice, significantly reduced from the 93% survival rate in the *It-map1*$^{+/+}$ mice (Fig. 6*e*). Thus, with two different precipitants of pancreatitis, deficiency of Itmap1 results in greater disease severity.

To gain further insight into the mechanism by which Itmap1 limited the severity of disease, we evaluated trypsin activation during the course of cerulein-induced pancreatitis. Both trypsinogen-activation peptide (TAP) concentration and trypsin activity were measured (Fig. 7, *a* and *b*). In the pancreas from wild type mice, both TAP and trypsin increased above background by 2 h after the initial cerulein injection. A smaller rise in TAP and trypsin was seen in the pancreas from *Itmap1*$^{-/-}$ mice. The difference between the TAP levels of the *Itmap1*$^{+/+}$ and *Itmap1*$^{-/-}$ mice was statistically significant at 8 h ($p = 0.002$). The differences between trypsin levels were statistically significant at 2 h ($p = 0.002$) and 8 h ($p = 0.001$). The difference in activated trypsin was not due to lower amounts of trypsinogen in the pancreas at baseline (*Itmap1*$^{+/+}$ 0.42 ± 0.08 and *Itmap1*$^{-/-}$ 0.47 ± 0.07 relative absorbance/ mg of protein) or 8 h after cerulein administration (*Itmap1*$^{+/+}$ 0.79 ± 0.11 and *Itmap1*$^{-/-}$ 0.84 ± 0.06 relative absorbance/mg of protein). There was also no difference in pancreatic cathepsin B content in the pancreas between genotypes at baseline (*Itmap1*$^{+/+}$ 0.94 ± 0.06 and *Itmap1*$^{-/-}$ 0.84 + 0.05 relative units/mg of protein) or 8 h after cerulein administration (*Itmap1*$^{+/+}$ 0.80 ± 0.05 and *Itmap1*$^{-/-}$ 0.80 ± 0.07 relative units/mg of protein).

We next measured myeloperoxidase (MPO) activity to assess the effect of Itmap1 deficiency on leukocyte infiltration during pancreatitis. The induction of pancreatitis was associated with an increase in MPO activity in the pancreas, but there was no difference in the MPO levels observed in pancreas of the *It-map1*$^{+/+}$ and *Itmap1* mice (Fig. 7*c*). This finding suggests that Itmap1 does not dampen the inflammatory response in acute pancreatitis.

Our above analyses of trypsin activity and TAP production suggest that Itmap1 does not protect against pancreatitis by limiting the activation of trypsin but, instead, is essential for normal trypsin activation. One testable hypothesis for how Itmap1 regulates trypsin activation and modifies the course of pancreatitis is that Itmap1 plays a role in sorting proteins into the zymogen granule. Lectin staining of zymogen granule membranes revealed no alteration in zymogen granule membrane glycoproteins in *Itmap1*$^{-/-}$ mice other than Itmap1 itself (data not shown). To determine if Itmap1 deficiency alters the composition of

zymogen granule contents, we performed proteomic analyses comparing contents of isolated *Itmap1*$^{+/+}$ and *Itmap1*$^{-/-}$ zymogen granules. Two-dimensional acrylamide gel electrophoresis (Fig. 8) followed by densitometric analysis (data not shown) of replicate stained gels for each genotype revealed an identical spectrum and relative abundance of detectable proteins between genotypes.

DISCUSSION

Our findings identify several important biological properties of Itmap1 and provide information about the *in vivo* function of this novel ZP and CUB domain protein. To date, the pancreas and the pregnant uterus are the only known sites of Itmap1 expression. In both organs, immunohistochemistry with anti-Itmap1 antibodies localized Itmap1 to cytoplasmic granules. Additional analysis of zymogen granule membranes from pancreatic acinar cells confirmed the presence of Itmap1 on these membranes. The inability to remove Itmap1 from zymogen granule membranes with high salt and alkali washes demonstrated tight association of Itmap1 with these membranes. Itmap1 is likely to be an integral membrane protein that is associated with the membrane through a putative transmembrane domain near the carboxyl terminus of the predicted protein sequence, although glycosylphosphatidylinositol linkage has not been excluded. Furthermore, Itmap1 is oriented such that the CUB and ZP domains are within the zymogen granule. Although Itmap1 was initially identified as a protein induced in late gestation mouse uterus (6), implicating it in the maintenance of pregnancy or progression of labor, we find no overt consequence of Itmap1 loss during pregnancy. In contrast, we showed that Itmap1 alters the course of acute pancreatitis induced by cerulein hyperstimulation or by a CDE diet. The largest effect was found in the CDE diet model of necrotizing pancreatitis. In this model, the mortality of the Itmap1-deficient mice increased almost 7-fold.

To define the mechanism by which Itmap1 protects against pancreatitis, we evaluated apoptotic cell death, leukocyte influx, and trypsinogen activation in the cerulein-hyperstimulated pancreas. Measurement of myeloperoxidase activity and evaluation of pancreatic histology indicate that Itmap1 deficiency does not predispose to exaggerated mononuclear cell invasion or sequestration during pancreatitis. Thus, Itmap1 probably does not function by dampening the inflammatory response in the pancreas, and it is not likely that Itmap1 deficiency is associated with altered NFκB activation, another presumed major determinant of experimental pancreatitis. We do find that Itmap1 deficiency increases the susceptibility of the acinar cell to apoptotic cell death. Increased cell death due to apoptosis would be expected to provide little additional inflammatory stimulus and may explain the equivalence of inflammatory markers between genotypes in the cerulein hyperstimulation model. Surprisingly, measurements of both trypsin activity and TAP revealed that *Itmap1*$^{-/-}$ mice had significantly less trypsinogen activation than did *Itmap1*$^{+/+}$ mice. This decrease in trypsin activation is not due to less trypsinogen within zymogen granules, because Western blot analysis of zymogen granule contents reveals similar amounts in normal and Itmap1-deficient mice. This finding shows that Itmap1 does not protect the pancreas by decreasing trypsin activation or activity when pancreatitis is induced.

The decreased trypsinogen activation in the face of more severe pancreatitis raises questions about the contribution of trypsin to the course of cerulein-induced pancreatitis. It has been generally assumed that pancreatitis is associated with a gain of trypsin function, but some have argued that the activation of trypsin during pancreatitis is protective against the action of other, more deleterious digestive enzymes (27). Our results add credence to the hypothesis that trypsin activation serves as a protective mechanism during acute pancreatitis. Although in cathepsin B-deficient mice decreased trypsinogen activation correlated with some parameters indicating less severe cerulein-induced pancreatitis (4), pancreatic

inflammation demonstrated little or no change. The unchanged inflammation in the cathepsin B-deficient mice, in accord with our findings, dissociates the trypsin activation from pancreatic inflammation. The greater severity of pancreatitis we find with Itmap1 deficiency may be due to the compartment in which cathepsin B modulates trypsinogen activation differing from that of Itmap1. Cathepsin B activates trypsinogen in vacuoles newly formed during hyperstimulation containing a mixture of zymogens and lysosomal hydrolases, whereas Itmap1 localizes to zymogen granules and is most likely to modulate trypsinogen activation within the zymogen granule itself. Our results underscore the complexity of the mechanisms involved in protecting the pancreas against damage and the initial events that trigger pancreatitis.

The location and structure of Itmap1 further suggest possible roles for this zymogen membrane protein. A submembranous matrix of proteoglycans resides on the inner surface of the zymogen granule membrane. It consists predominantly of poorly characterized proteoglycans, although the most abundant component, Muclin, has been described (28). Muclin, a 300-kDa glycoprotein, with sulfated *O*-linked carbohydrate chains is, like Itmap1, a ZP domain protein. The major glycoprotein of the zymogen granule membrane, GP2, links with the proteoglycans of the submembranous matrix and helps keep them tightly associated with the membrane (29). Interestingly, GP2 is also a ZP domain-containing protein (30, 31). By analogy to other ZP domain proteins, we propose that Itmap1 interacts with the submembranous fibrillar ZP domain matrix where it may contribute to zymogen assembly or stability. Given the finding that the distribution and relative abundance of components of zymogen granule contents does not differ between $Itmap1^{+/+}$ and $Itmap1^{-/-}$ mice, it is unlikely that Itmap1 plays an important role in the sorting of proteins into the zymogen granule. Further studies designed to elucidate the role of Itmap1 in zymogen granule stability and trypsin activation are in progress.

We have described a new pancreatic glycoprotein that is present on zymogen granule membranes. Importantly, although the full spectrum of its actions may not yet be defined, Itmap1 significantly attenuates the course of acute pancreatitis in mice. Because Itmap1 is also expressed in the human pancreas,[2] dysregulation of Itmap1 expression may contribute to variation in susceptibility to pancreatitis after toxin exposure, *e.g.* alcohol abuse, and in genetic diseases such as cystic fibrosis. Future efforts will be essential to determine the role of Itmap1 in human disease and whether modulation of Itmap1 activity will prove useful as a therapeutic intervention.

Acknowledgments

We thank Dr. John Kasik for providing the Itmap1 full-length cDNA and helpful discussions, Marilyn Levy for assistance with electron microscopy, and Drs. Jonathan Gitlin and David Alpers for manuscript review.

REFERENCES

1. Steinberg W, Tenner S. N. Engl. J. Med. 1994; 330:1198–1210. [PubMed: 7811319]
2. Bettinger JR, Grendell JH. Pancreas. 1991; 8(Suppl 1):S2–S6. [PubMed: 1788248]
3. Whitcomb DC, Gorry MC, Preston RA, Furey W, Sossenheimer MJ, Ulrich CD, Martin SP, Gates LK, Amann ST, Toskes PP, Liddle R, McGrath K, Uomo G, Post JC, Ehrlich GD. Nat. Genet. 1996; 14:141–145. [PubMed: 8841182]
4. Halangk W, Lerch MM, Brandt-Nedelev B, Roth W, Ruthenbuerger M, Reinheckel T, Domschke W, Lippert H, Peters C, Deussing J. J. Clin. Invest. 2000; 106:773–781. [PubMed: 10995788]

[2]M. E. Lowe and L. J. Muglia, unpublished data.

5. Steer, M. The Pancreas: Biology, Pathobiology, and Disease. Second Ed.. Go, V.; Dimagno, E.; Gardner, J.; Lebenthal, E.; Reber, H.; Scheele, G., editors. New York, NY: Raven Press; 1993. p. 581-591.
6. Kasik JW. Biochem. J. 1998; 330:947–950. [PubMed: 9480914]
7. Killick R, Legan P, Malenczak C, Richardson G. J. Cell Biol. 1995; 129:535–547. [PubMed: 7721949]
8. De Lisle RC, Ziemer D. Eur. J. Cell Biol. 2000; 79:892–904. [PubMed: 11152281]
9. Tybulewicz V, Crawford C, Jackson P, Bronson R, Mulligan R. Cell. 1991; 65:1153–1163. [PubMed: 2065352]
10. Deng C, Wynshaw-Boris A, Shen MM, Daugherty C, Ornitz DM, Leder P. Genes Dev. 1994; 8:3045–3057. [PubMed: 8001823]
11. Muglia LJ, Jenkins NA, Gilbert DJ, Copeland NG, Majzoub JA. J. Clin. Invest. 1994; 93:2066–2072. [PubMed: 8182138]
12. Muglia LM, Schaefer ML, Vogt SK, Gurtner G, Imamura A, Muglia LJ. J. Neurosci. 1999; 19:2051–2058. [PubMed: 10066258]
13. De Lisle RC, Schulz I, Tyrakowski T, Haase W, Hopfer U. Am. J. Physiol. 1984; 246:G411–G418. [PubMed: 6609646]
14. Wishart MJ, Andrews PC, Nichols R, Blevins GT, Logsdon CD, Williams JA. J. Biol. Chem. 1993; 268:10303–10311. [PubMed: 8486693]
15. Gross G, Imamura T, Vogt SK, Wozniak DF, Nelson DM, Sadovsky Y, Muglia LJ. Am. J. Physiol. 2000; 278:R1415–R1423.
16. Christie DL, Palmer DJ. Biochem. J. 1990; 270:57–61. [PubMed: 2396993]
17. Lampel M, Kern HF. Virch. Arch. A Pathol. Anat. Histol. 1977; 373:97–117.
18. Adler G, Hupp T, Kern HF. Virch. Arch. A Pathol. Anat. Histol. 1979; 382:31–47.
19. Niederau C, Niederau M, Luthen R, Strohmeyer G, Ferrell LD, Grendell JH. Gastroenterology. 1990; 99:1120–1127. [PubMed: 2394333]
20. McDonald MK, Ellis S. Life Sci. 1975; 17:1269–1276. [PubMed: 577]
21. Jaffrey C, Eichenbaum D, Denham DW, Norman J. Pancreas. 1999; 19:377–381. [PubMed: 10547198]
22. Lombardi B, Rao NK. Am. J. Pathol. 1975; 81:87–99. [PubMed: 1180334]
23. Lombardi B, Estes LW, Longnecker DS. Am. J. Pathol. 1975; 79:465–480. [PubMed: 1094837]
24. Thim L, Mortz E. Regulatory Peptides. 2000; 90:61–68. [PubMed: 10828494]
25. Mashimo H, Wu DC, Podolsky DK, Fishman MC. Science. 1996; 274:262–265. [PubMed: 8824194]
26. Rao KN, Tuma J, Lombardi B. Gastroenterology. 1976; 70:720–726. [PubMed: 1261763]
27. Lerch MM, Gorelick FS. Med. Clinics N. Am. 2000; 84:549–563.
28. De Lisle RC. J. Cell. Biochem. 1994; 56:385–396. [PubMed: 7876332]
29. Freedman SD, Scheele GA. Eur. J. Cell Biol. 1993; 61:229–238. [PubMed: 8223713]
30. Hoops TC, Rindler MJ. J. Biol. Chem. 1991; 266:4257–4263. [PubMed: 1999417]
31. Fukuoka S, Freedman SD, Scheele GA. Proc. Natl. Acad. Sci. U. S. A. 1991; 88:2898–2902. [PubMed: 2011597]

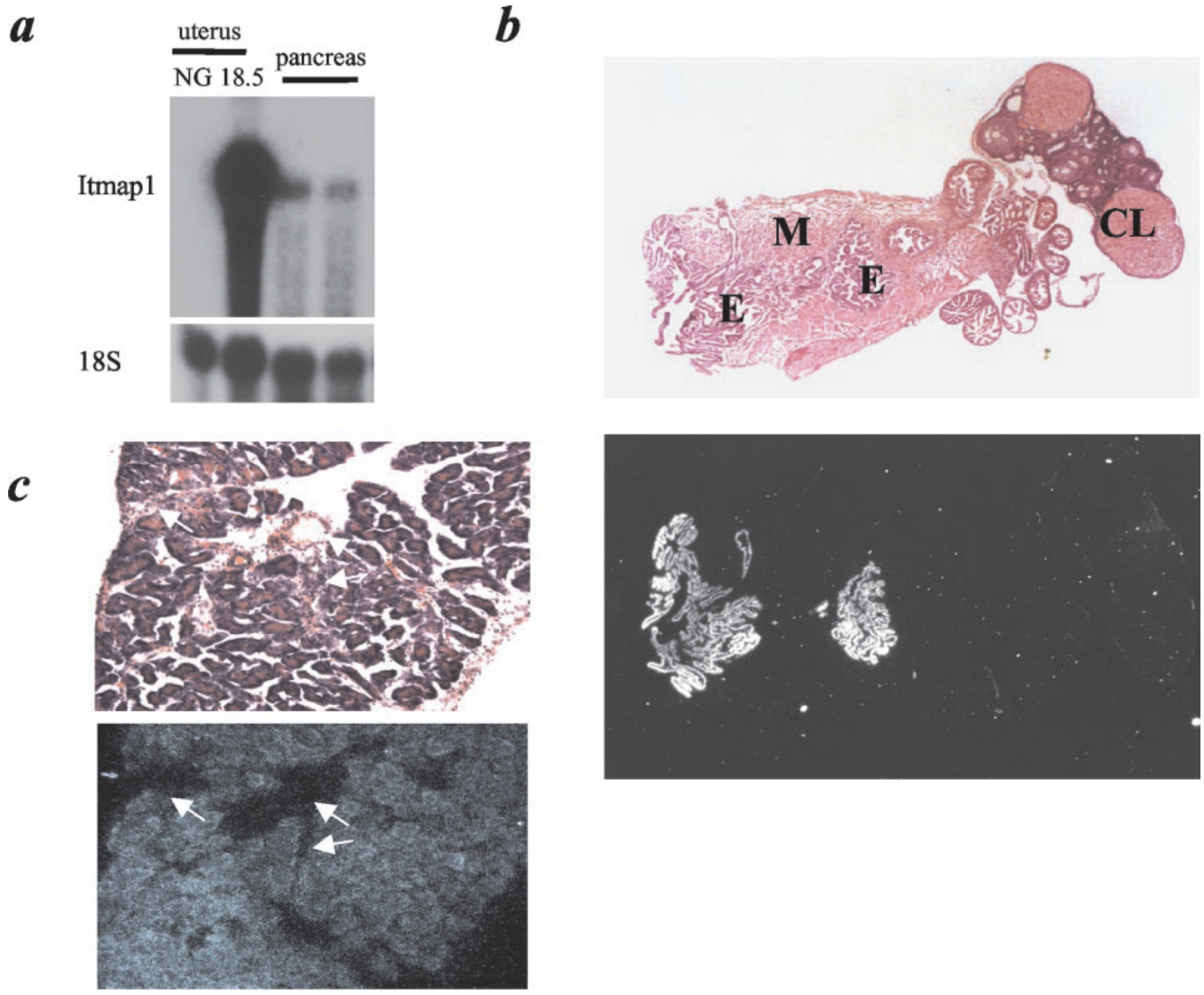

Fig. 1. Expression of Itmap1 in the pancreas and uterus

*a*Northern blot analysis. Total cellular RNA from non-gravid (*NG*) and 18.5-day gestation uterus and two adult pancreata was hybridized to either an Itmap1 probe or an 18 S ribosomal RNA probe to control for sample loading and recovery. *b, in situ* hybridization localization of Itmap1 mRNA in day 16 gestation uterus. The *upper panel* demonstrates the locations of the uterine endometrium (*E*) and myometrium (*M*), and ovarian corpus luteum (*CL*) on a hematoxylin and eosin-stained section. Silver deposition viewed by dark field microscopy reveals restriction of Itmap1 mRNA to the endometrium (*lower panel*). *c, in situ* hybridization localization of Itmap1 mRNA in the pancreas (*upper panel*, hematoxylin and eosin-stained frozen section; *lower panel*, dark field). Itmap1 hybridization occurs throughout the acinar cell population but not the ductal cells (indicated by the *arrows*).

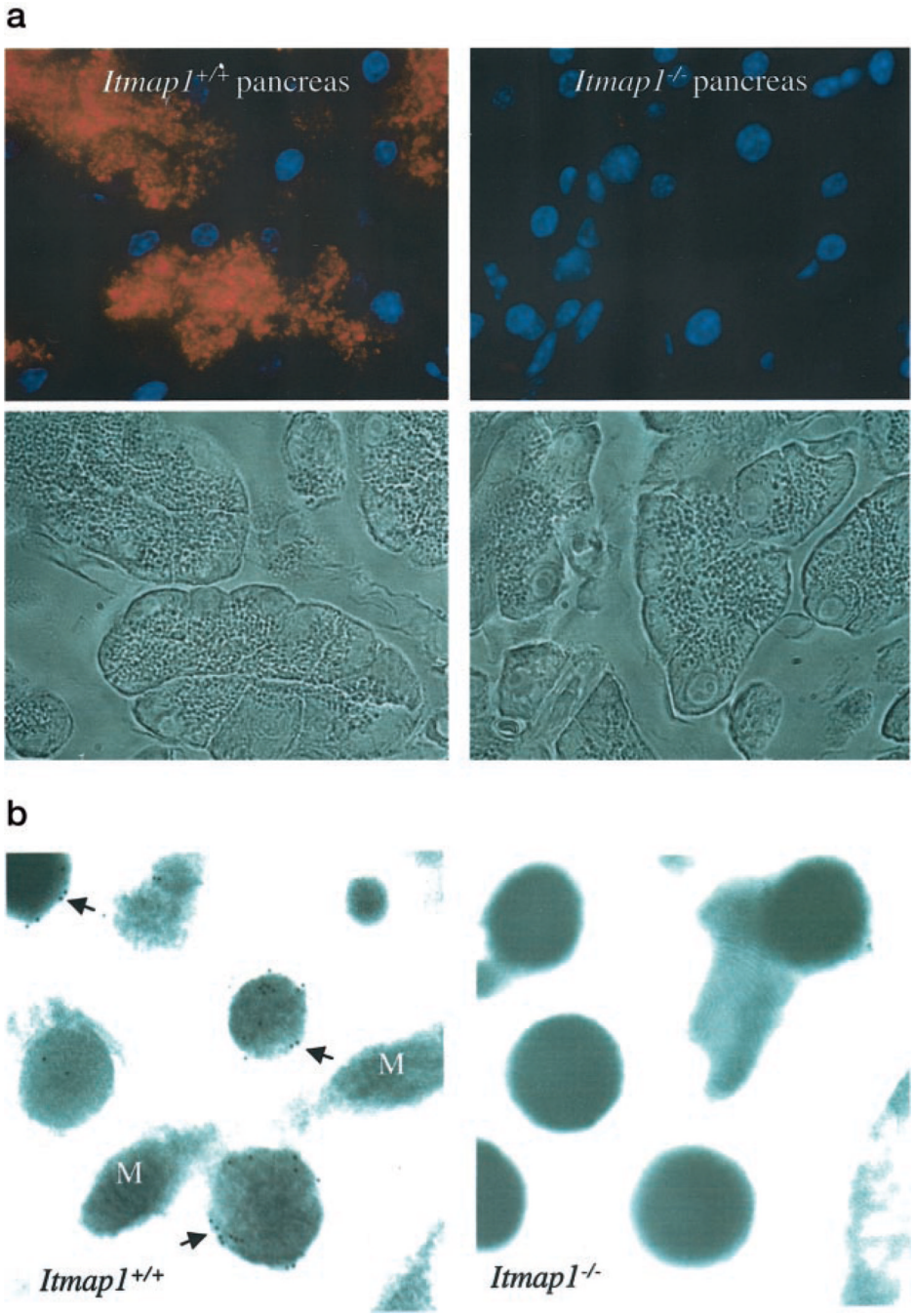

Fig. 2. Immunohistochemical localization of Itmap1

a, Itmap1 immunore-activity (*upper panels, orange*) was detected with a rabbit polyclonal anti-Itmap1 anti-serum in *Itmap1*$^{+/+}$, but not *Itmap1*$^{-/-}$, zymogen granules within the pancreas (*lower panels, phase-contrast image*). Sections were counterstained with 4',6-diamidino-2-phenylindole for localization of nuclei (*blue*). Magnification, ×100. *b*, immunoelectron microscopic detection of Itmap1 immunoreactivity in zymogen granules of *Itmap1*$^{+/+}$ mice. Deposition of immunogold beads is noted predominantly on the zymogen granule membrane (*arrows*). Mitochondria (*M*) are unstained.

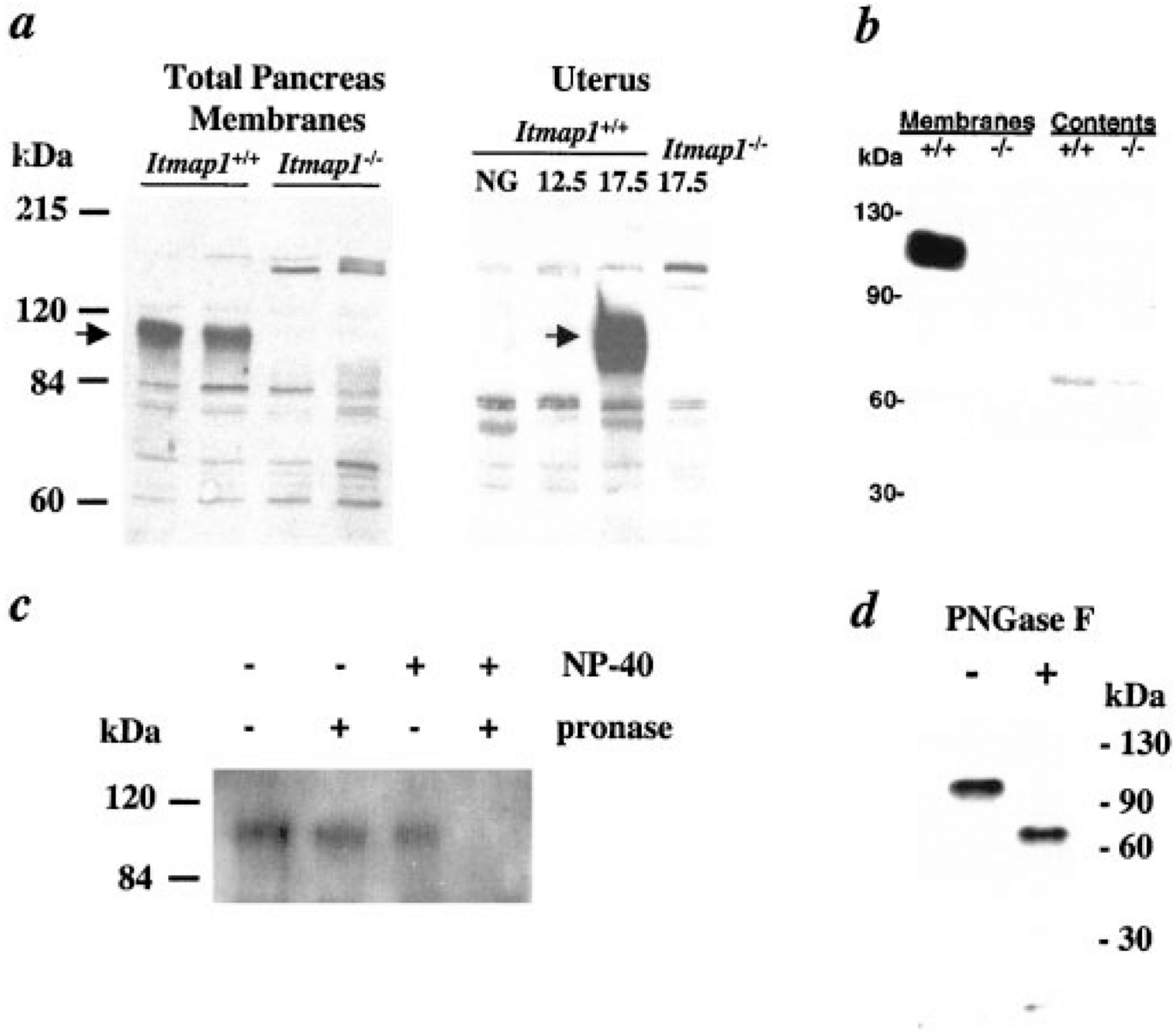

Fig. 3. Western blot analysis of Itmap1

a, detection of Itmap1 in pancreatic or uterine total membrane proteins. An immunoreactive protein of ~110 kDa (*arrow*) is found in *Itmap1*$^{+/+}$, but not *Itmap1*$^{-/-}$, total membrane protein extracts. *b*, detection of Itmap1 in zymogen granule membranes, but not zymogen granule contents, of *Itmap1*$^{+/+}$ mice. Equivalent loading of zymogen granule proteins was confirmed by Ponceau S membranes and lectin binding (not shown). *c*, orientation of Itmap1 in the zymogen granule. Western blot analysis of Itmap1 in isolated zymogen granules with and without protease (Pronase) and detergent (Nonidet P-40) treatment. Itmap1 immunoreactivity is abolished with protease treatment only when zymogen granules are perme-abilized with Nonidet P-40. *d*, Western blot analysis of Itmap1 with and without digestion of zymogen granule membrane glycoproteins with peptide: *N*-glycosidase F (*PNGase F*). Reduction in size of the Itmap1 immunoreactive band to a molecular weight consistent with the translated cDNA is observed.

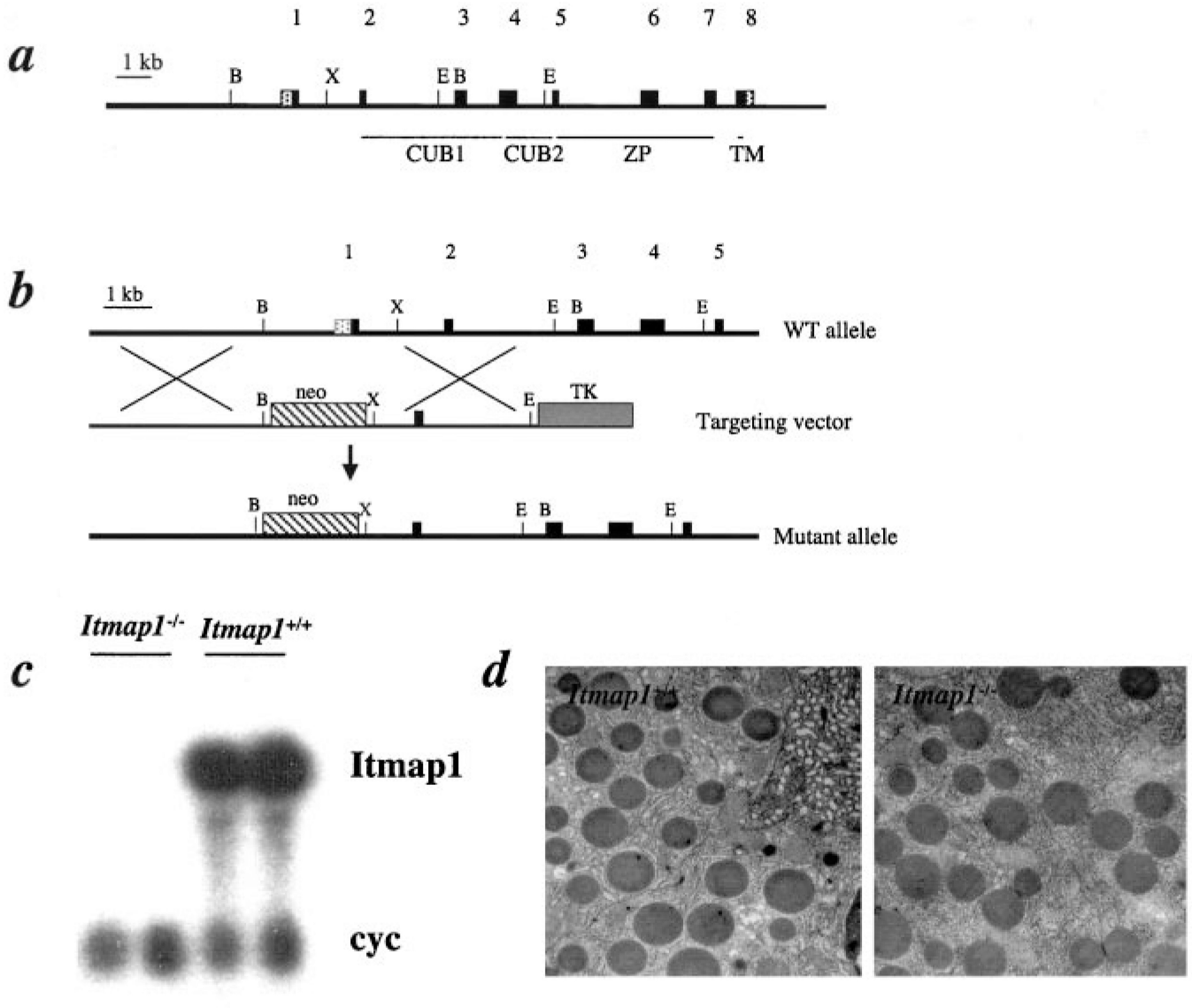

Fig. 4. Targeted inactivation of *Itmap1*

a, structure of the *Itmap1* gene. Exons are indicated by *boxes*, with the untranslated regions *stippled*. Regions coding for the CUB, zona pellucida (*ZP*), and putative transmembrane (*TM*) domains are indicated. A subset of restriction sites is shown for relative orientation. *B, BamH*I; *X, Xba*I; *E, EcoR*I. *b*, strategy for homologous recombination. Exon 1 and a portion of the 5'-flanking region are replaced by a neomycin (*neo*) selection cassette. A herpes simplex virus thymidine kinase (*TK*) cassette was also included in the targeting vector to provide negative selection. *WT*, wild type. *c*, Northern blot analysis of total day-18.5 gestation uterine RNA from $Itmap1^{-/-}$ and $Itmap1^{+/+}$ mice hybridized to Itmap1 and cyclophilin (*cyc*) antisense riboprobes. *d*, electron microscopic analysis of zymogen granules. Magnification, ×7000.

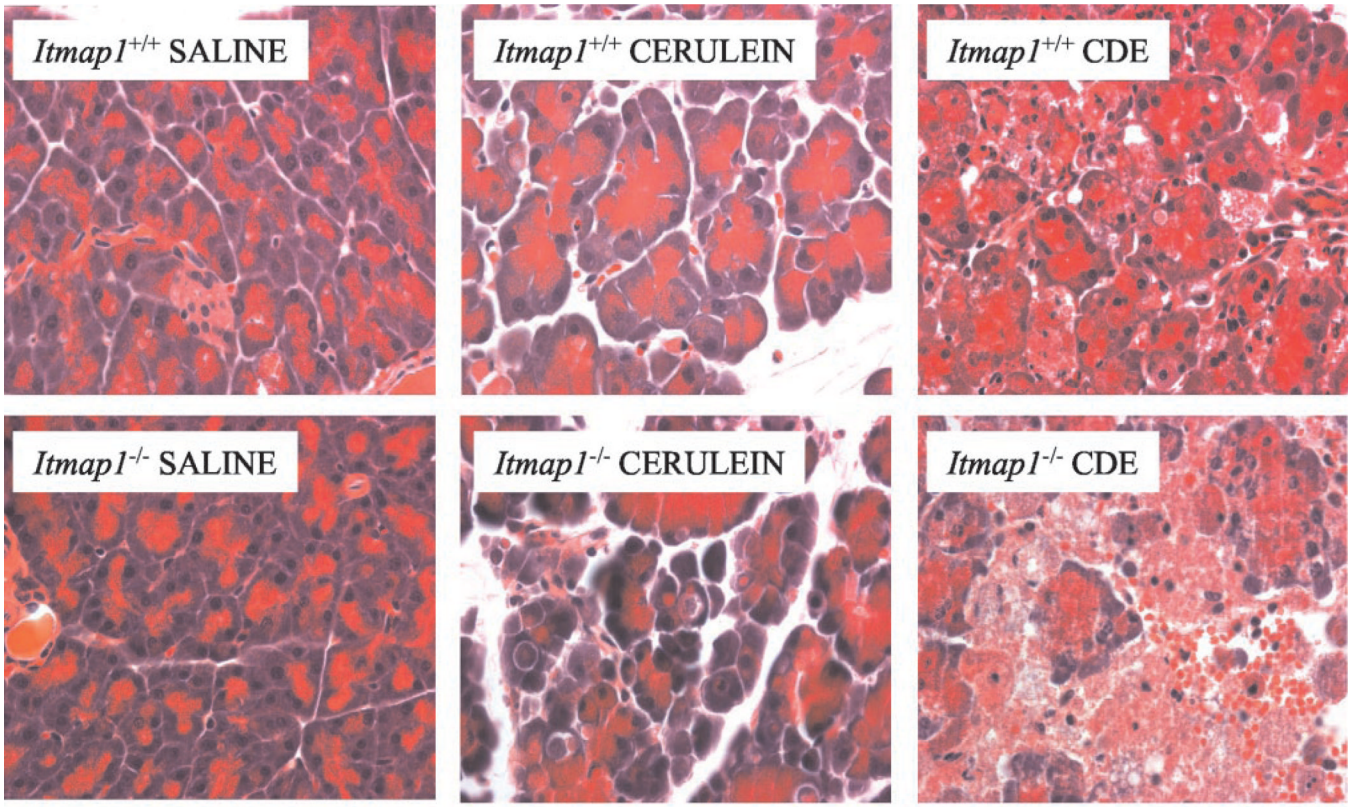

Fig. 5. Pancreatic histology during pancreatitis in *Itmap1*$^{+/+}$ and *Itmap1*$^{-/-}$ mice

Representative hematoxylin and eosin-stained paraffin sections of control saline-injected, cerulein-injected, and choline-deficient, ethionine-supplemented (CDE)-diet-treated mice. Edema is visualized as increased intralobular separation in cerulein and CDE groups. Prominent cellular necrosis is found in the *Itmap1*$^{-/-}$ CDE group.

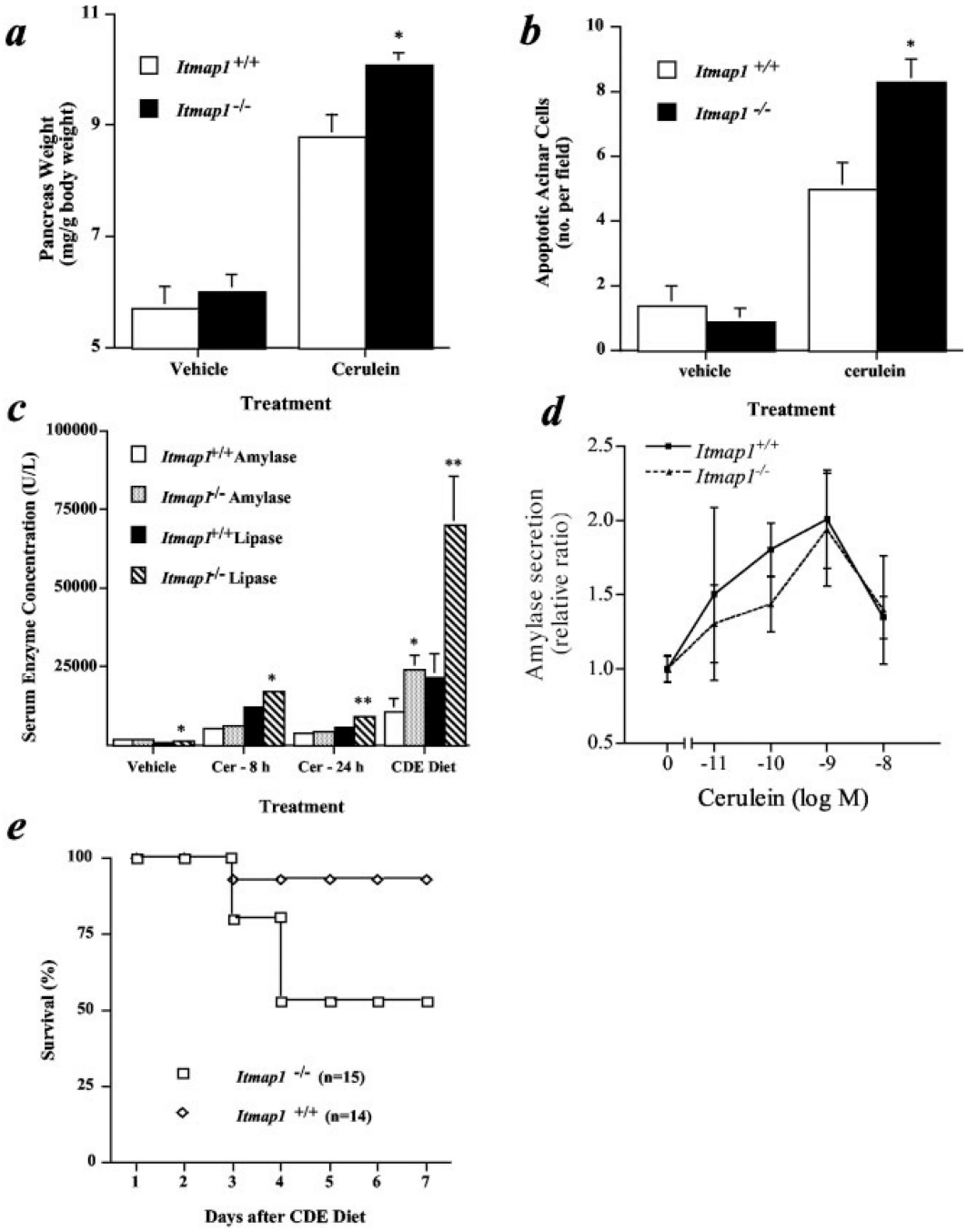

Fig. 6. Sequelae of pancreatitis in *Itmap1*$^{+/+}$ and *Itmap1*$^{-/-}$ mice

a, pancreatic weight during cerulein-induced pancreatitis. *, $p < 0.05$ *versus* cerulein-treated *Itmap1*$^{+/+}$ mice. *b*, induction acinar cell apoptosis during cerulein-induced pancreatitis. Number of TUNEL-positive acinar cells per ×400 magnification field is shown as a function of treatment and genotype. *, $p < 0.05$ *versus* cerulein-treated *Itmap1*$^{+/+}$ mice. *c*, serum amylase and lipase measurement during cerulein and CDE-diet pancreatitis. *,$p < 0.05$; **, $p \leq 0.01$ versus *Itmap1*$^{+/+}$ enzyme group at same time point. *d*, cerulein concentration dependence of amylase secretion from pancreatic snips in *Itmap1*$^{+/+}$ and *Itmap1*$^{-/-}$ mice. Amylase released into the media after the addition of cerulein for 30 min is shown normalized to the vehicle controls. Mean ± S.E. is displayed from triplicate samples for each

concentration and genotype. Differences between genotypes were not statistically significant. *e*, survival curve with CDE diet. Overall survival significantly differed between *Itmap1*$^{+/+}$ and *Itmap1*$^{-/-}$ mice ($p < 0.05$).

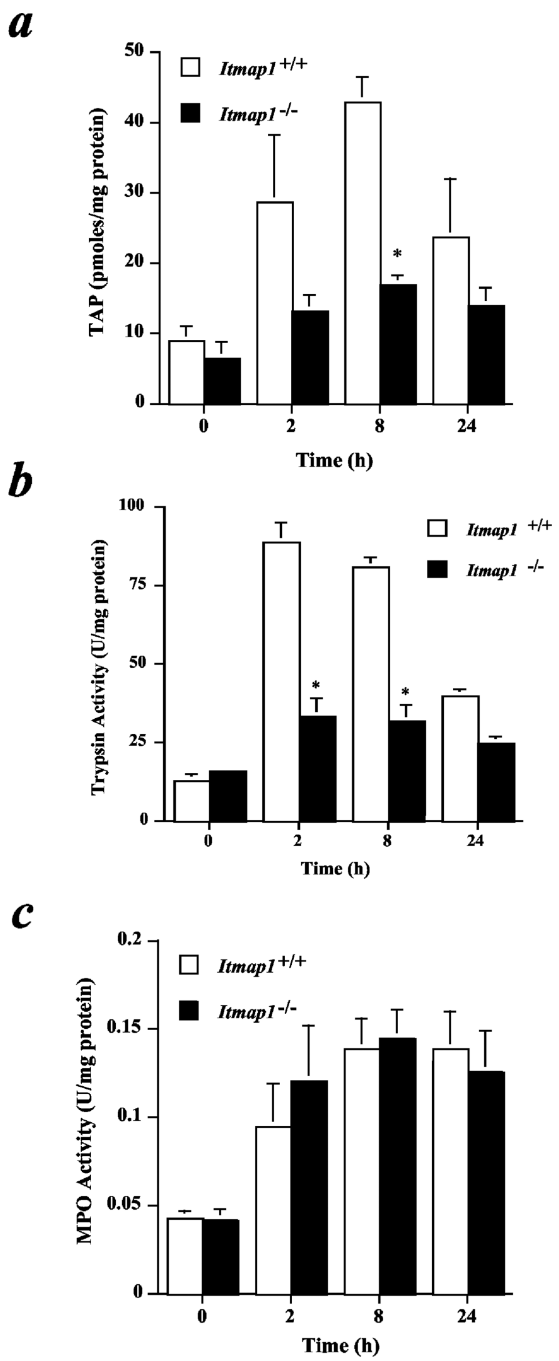

Fig. 7. Trypsin activation and inflammatory cell infiltration in during cerulein-induced pancreatitis in *Itmap1*$^{+/+}$ and *It-map1*$^{-/-}$ mice

Time course of TAP production (*a*), trypsin activity (*b*), and myeloperoxidase activity (*c*), in the pancreas after initiation of cerulein injections at time zero. *, $p < 0.005$.

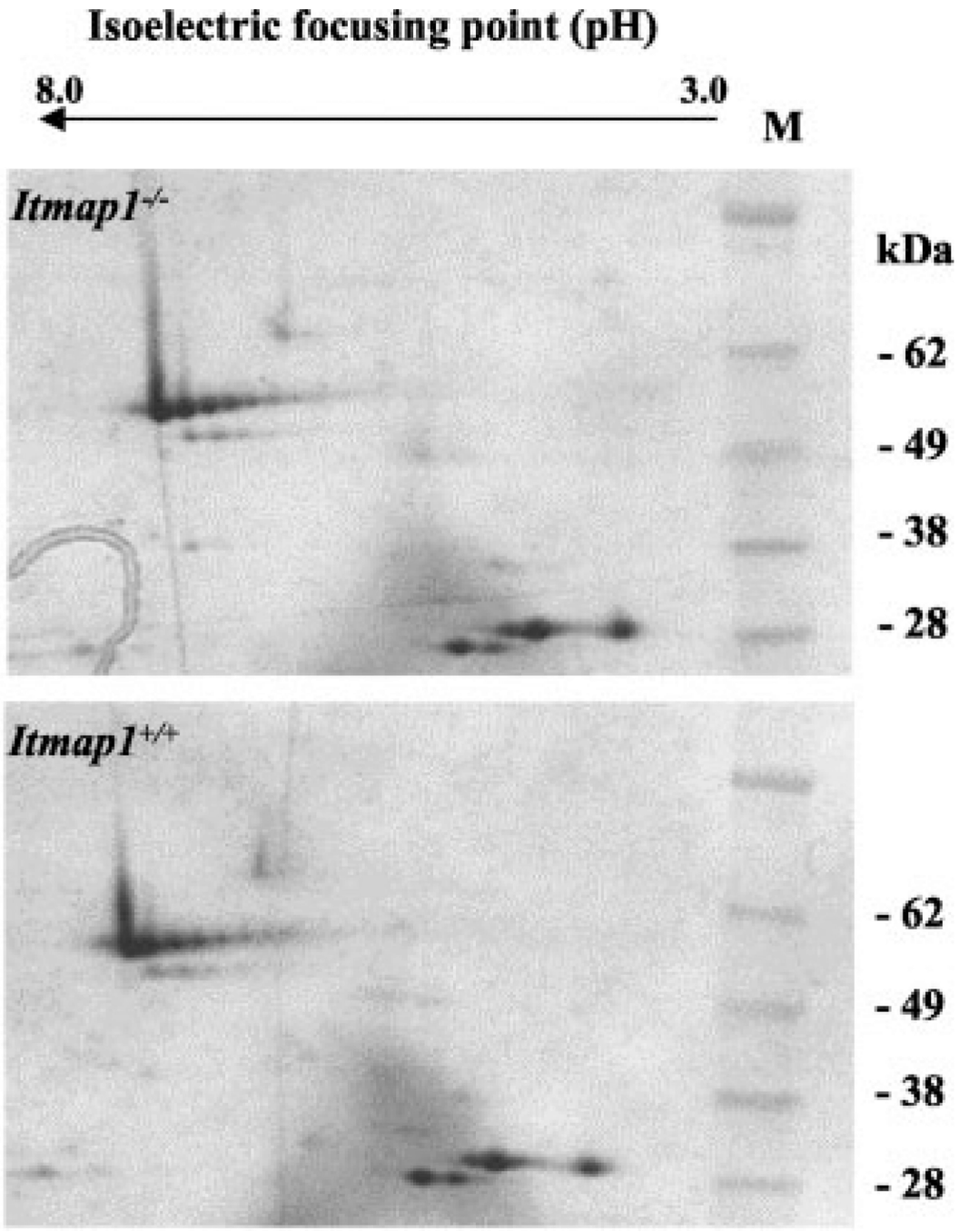

Fig. 8. Proteomic analysis of isolated zymogen granule contents

First-dimension separation of granule contents proteins was performed on isoelectric focusing strips. The focused samples were then loaded onto 4–12% gradient acrylamide gels for second-dimension separation by SDS-PAGE on the basis of size. Shown are representative Coomassie Brilliant Blue G-colloidal-stained gels of granule contents of each genotype. *M*, molecular weight ladder.